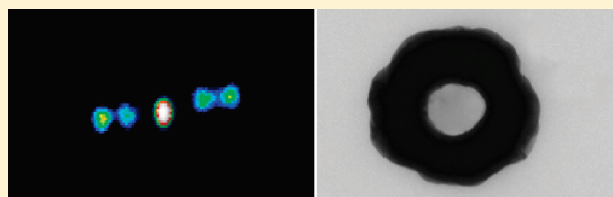


# Spatially Modulated Two-Photon Luminescence from Si–Au Core–Shell Nanowires

Nan Lin,<sup>†</sup> Weixia Zhang,<sup>‡</sup> Brooke M. Koshel,<sup>‡</sup> Ji-Xin Cheng,<sup>†,‡,\*</sup> and Chen Yang<sup>‡,§,\*</sup><sup>†</sup>Weldon School of Biomedical Engineering, Purdue University, West Lafayette, Indiana 47907, United States<sup>‡</sup>Department of Chemistry, Purdue University, West Lafayette, Indiana 47907, United States<sup>§</sup>Department of Physics, Purdue University, West Lafayette, Indiana 47907, United States

**ABSTRACT:** Si–Au core–shell nanowires were synthesized with a two-step strategy combining chemical vapor deposition and wet chemistry methods. Si core diameter, Au shell thickness, and wire length were controlled during synthesis. Under a far-field two-photon excitation scanning microscope, spatially modulated two-photon luminescence (TPL) was observed from the core–shell nanowires prepared with several micrometers in length. The mode spacing scales linearly with the length of nanowires for samples with 15 and 40 nm Au shells. The spatial modulation pattern was found to be independent of the excitation wavelength. The TPL intensity displayed a  $\cos^2$  dependence on the excitation field polarization, indicating a sequential two-photon excitation process enhanced by the longitudinal plasmon field. The spatially modulated TPL is interpreted by a standing wave model of surface plasmon polaritons along the core–shell nanowire which acts as a Fabry–Pérot resonator. These results suggest TPL imaging of Si–Au core–shell nanowires as a new system providing useful insights regarding a plasmonic wave in a 1-D nanostructure.



## INTRODUCTION

First discovered by Mooradian<sup>1</sup> in 1969, the photoluminescence of a noble metal originates from recombination of free electrons in the sp band and the holes in the d band and can be amplified by several orders of magnitude by coupling of the plasmonic field.<sup>2,3</sup> The plasmonic field also enhances two-photon absorption, resulting in an intense two-photon luminescence (TPL) observed in gold nanorod,<sup>4</sup> nanoshell,<sup>5</sup> and nanowire.<sup>6</sup> The TPL signal has been used as a readout of plasmonic field strength in gap antenna<sup>7</sup> and bow-tie structure.<sup>8</sup> Using scanning near-field optical microscopy (SNOM),<sup>9,10</sup> Imura et al. found that a single gold nanorod several hundred nanometers in length displayed spatially modulated TPL signals which were attributed to the local density of states of the surface plasmon wave. Indeed, Ditlbacher et al.<sup>11</sup> and Dorfmueller et al.<sup>12</sup> also reported spatially modulated patterns attributed to Fabry–Pérot resonance in SNOM images. Studies were performed on silver nanowires produced through a chemical reaction in aqueous electrolyte and Au nanostructures fabricated by e-beam lithography. Although these existing metal nanomaterials have been used as testing systems to produce exciting results, low aspect ratio in Au nanorods, instability of electrolyte-produced Ag nanowires in air,<sup>13</sup> fixed rectangular cross-section, and potential surface roughness in e-beam-fabricated Au nanowires can limit their use for further systematic studies on the properties of plasmonic waves in metal nanostructures.<sup>11,12,14–18</sup>

To this end, we developed a new group of stable nanomaterials, Si–Au core–shell nanowires, with a smooth surface, a unique geometry, and complete control of dimensions. The Si–Au

core–shell nanowires, in which silicon cores were completely wrapped around by a coaxial Au layer, were synthesized using a two-step strategy. The chemical vapor deposition method, the first step, enabled control of core diameter and wire length for the silicon core, and the second step, wet chemistry, allowed control of gold shell thickness. Compared to metal/semiconductor core–shell nanowires previously produced by thermal or e-beam evaporation of metal coating on free-standing nanowires grown on the substrate, shell growth in our method is produced by the reduction reaction in aqueous solution. Such growth provides controllable and slow coating initiated by nanoscale nucleation sites, therefore offering more uniform and smoother shells. Such improvements on the shell structures can be critical to enable observation and study of surface plasmon-related phenomena. We observed a spatially modulated TPL signal under a far field detection condition from the core–shell nanowires with micrometer lengths. Such TPL signals were further characterized when varying wire length, Au shell thickness, excitation wavelength, and excitation polarization.

## EXPERIMENTAL METHODS

**Core–Shell Nanowire Synthesis.** The synthesis scheme of Si–Au core–shell nanowires is illustrated in Figure 1a. Silicon nanowires (SiNWs) were first synthesized on an Al<sub>2</sub>O<sub>3</sub> substrate

Received: August 20, 2010

Revised: January 3, 2011

Published: February 04, 2011

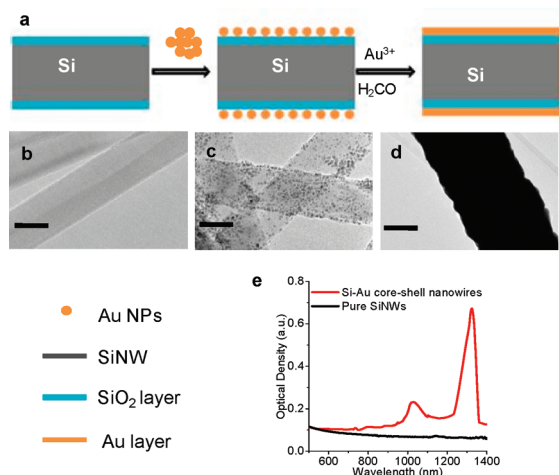


**Figure 1.** Synthesis and optical properties of Si–Au core–shell nanowires. (a) Schematic of key synthesis steps. (b) TEM image of SiNWs. (c) TEM image of Au nanoparticle-decorated SiNWs. (d) TEM image of a Si–Au core–shell nanowire. Scale bars are 30 nm. (e) Extinction spectra of SiNWs (black) and Si–Au core–shell nanowires (red) with 40 nm Si core and 15 nm Au shell. Both samples have average 3.1  $\mu\text{m}$  lengths.

using a Au nanoparticle-mediated chemical vapor deposition method.<sup>19</sup> Formation of the shell is similar to the shell formation in the Si–Au nanoshell synthesis developed by the Halas group.<sup>20</sup> Specifically, the  $\text{Al}_2\text{O}_3$  growth substrate containing a high yield of free-standing SiNWs was first treated with oxygen plasma to create a thin and uniform oxidized layer on the surface of SiNWs. The SiNW surface was then modified by immersing the growth substrate in 10% 3-aminopropyltrimethoxysilane (APTMS) in ethanol for at least 24 h. To further enhance covalent bonding of the APTMS group, the 10% APTMS solution in ethanol with the  $\text{Al}_2\text{O}_3$  substrate inside was boiled for at least another 2 h.<sup>21</sup> The  $\text{Al}_2\text{O}_3$  substrate was then rinsed with pure ethanol to remove excess APTMS before further use.

Gold nanoparticles with diameters of 1–3 nm and a net negative surface charge were prepared separately using the reduction of chloroauric acid with tetrakis(hydroxymethyl) phosphonium chloride (THPC).<sup>22</sup> The APTMS-treated growth substrate was then immersed into the Au nanoparticle solution for at least 24 h to enable attachment of Au nanoparticles onto the surface of SiNWs. Unattached Au nanoparticles were removed, and the Au particle-decorated SiNWs were then removed from the substrates and dispersed to 1 mL of HPLC-grade water by a brief sonication.

A reducible gold solution was used to grow a gold layer on the Au particle-decorated SiNWs. To prepare the reducible gold solution 25 mg (1.8 mmol) of potassium carbonate ( $\text{K}_2\text{CO}_3$ ) was dissolved in 100 mL of HPLC-grade water. The potassium carbonate solution was under strong vortex for 10 min, and then 2.0 mL (0.29 mmol) of 1%  $\text{HAuCl}_4$  solution was added. To a vigorously stirred 2 mL aliquot of the reduction solution, 1 mL of Au/APTMS/SiNWs was added. After stirring the solution for 10 min, a 10  $\mu\text{L}$  (0.36 mmol) aliquot of formaldehyde was quickly added.<sup>20</sup> Over the course of 10 min, some dark brown precipitations appeared at the bottom of the reaction flask, which indicates formation of the core–shell structure.

**Two-Photon Luminescence Imaging.** Nonlinear optical properties of the Si–Au core–shell nanowires dispersed on a

coverslip were studied using a multimodal multiphoton scanning microscope.<sup>23</sup> A femtosecond laser of 80 MHz repetition rate and 130 fs pulse width (Mai Tai, Spectra-Physics) was used as the source of optical excitation. The Mai Tai laser beam was sent to an inverted confocal microscope (FV1000+IX81, Olympus America Inc.). A 60 $\times$  water immersion objective with a 1.2 numerical aperture was used to focus the Mai Tai beam onto a sample. The transmission optical light was collected by a built-in internal PMT detector. The luminescence signal was collected by the same objective, separated from the excitation beam by a dichroic mirror (675dcspxr, Chroma), transmitted through a 380–680 nm band-pass filter, and detected by an external PMT detector (R7683, Hamamatsu Photonics).

## RESULTS AND DISCUSSION

This synthesis strategy combines the CVD method and wet chemistry, which enables independent control of key structural parameters of the Si–Au core–shell nanowire, such as core diameter, shell thickness, and wire length. SiNWs, Au nanoparticle-decorated SiNWs, and Si–Au core/shell nanowires were characterized by transmission electron microscopy (TEM). Corresponding TEM images are shown in Figure 1b–d. The diameter of the SiNW was measured to be approximately 40 nm (Figure 1b), consistent with the size of the Au nanoparticles initiating nanowire growth. The thickness of the Au layer is estimated to be 15 nm based on the measured total diameter from the Au–Si core–shell nanowires (Figure 1d) and the diameter of the Si core. This Au thickness can be further controlled by varying the volume of reduction solution while keeping other synthesis conditions fixed. The length of nanowires was controlled by growth time and pressure during CVD synthesis and was later measured in transmission images once dispersed on a coverslip.

To examine the effects of the Au shell on the optical properties of SiNWs, we recorded the extinction spectra (Jasco V570 UV/visible/NIR spectrophotometer) of both SiNW solution and core–shell nanowire solution in the spectral region from 500 nm to 1.4  $\mu\text{m}$  (Figure 1e). The average length of the nanowires measured was  $\sim 3.1 \mu\text{m}$  for both samples. In contrast to SiNWs, we observed a broad extinction profile in this wavelength range with two strong peaks at 1040 and 1330 nm from the core–shell nanowires. We hypothesize that the peak at 1330 nm is due to the plasmonic resonance of the Au shell on nanowires, which will be further confirmed by theoretical modeling of TPL signals from the core–shell structure.

The Si–Au core/shell nanowires were clearly visible in the transmission channel (Figure 2a). With an excitation at 850 nm using a femtosecond laser, we observed a bright luminescence from these wires (Figure 2b). Moreover, the luminescence signal showed a strong dependence on the nanowire orientation, being depleted when nanowire axes were perpendicular with the laser field polarization (circled in Figure 2b). A quadratic dependence of the signal intensity on the input power is confirmed by a slope value of 2.07 obtained from the linear fitting of a  $\log(\text{intensity})$  vs  $\log(\text{power})$  curve in Figure 2c, indicating that the luminescence was a result of two-photon excitation. We further recorded the two-photon luminescence (TPL) emission spectrum generated from a single nanowire (Figure 2d) using the  $\lambda$ -scan function of the microscope. The luminescence showed a broad spectral profile with a peak at approximately 480 nm.

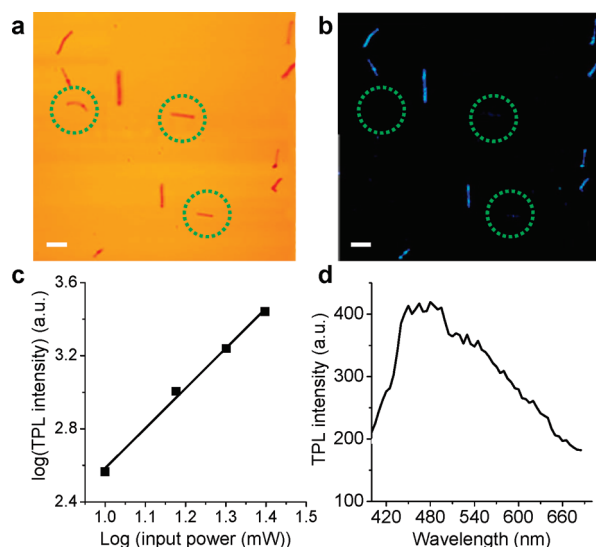


**Figure 2.** TPL from Si–Au core–shell nanowires. (a) Transmission image of Si–Au nanowires deposited on a coverslip. (b) TPL image of the same sample. Scale bars are  $3 \mu\text{m}$ . Dashed circles highlight the nanowires of which axes are perpendicular with the laser field polarization. (c) Power dependence measurement on a single Si–Au nanowire. The four data points are recorded when 10, 15, 20, and 25 mW power at the microscope was applied. The black line is the linear fit. (d) TPL emission spectrum. Excitation wavelength was 850 nm for c and d.

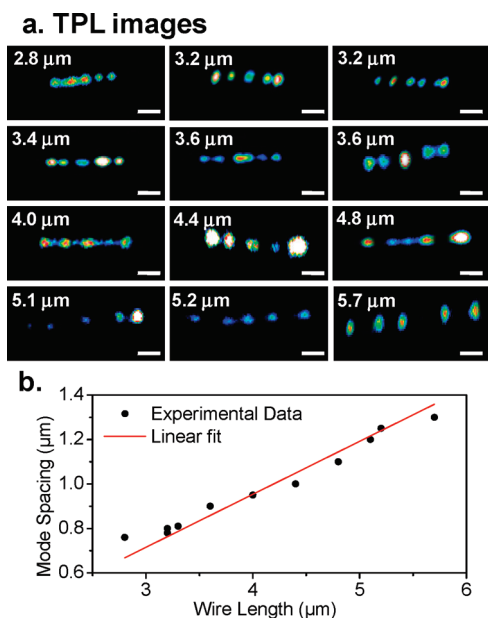


**Figure 3.** Spatially modulated TPL of Si–Au core–shell nanowires with 15 nm Au shell. (a) TPL images and intensity profiles of Si–Au core–shell nanowires. Excitation was at 850 nm, and the power at the sample was 1.0 mW. Scale bar is  $1 \mu\text{m}$ . (b) Mode spacing as a function of the length of Si–Au core–shell nanowires. The red curve is a linear fit with the function  $y = kx$ .

By zooming into individual nanowires, we observed that the TPL signal from these core–shell structures displayed alternative bright and dark patterns along the nanowire axes (Figure 3a–d). Although similar patterns of TPL were seen in gold nanorods of 330 nm in length,<sup>9,10</sup> the spatially modulated TPL along a single nanowire of a few micrometers in length

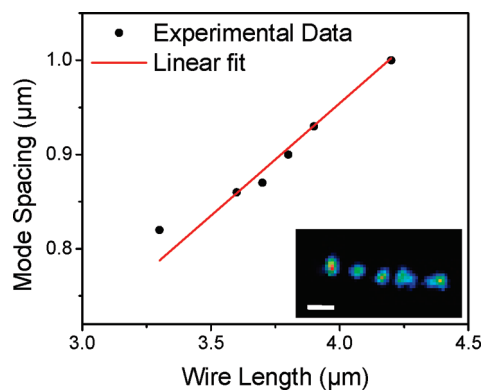


**Figure 4.** Mode spacing as a function of the length of nanowires with a 40 nm Au shell. A total of 6 wires were measured. The red curve is a linear fit with the function  $y = kx$ . (Inset) Spatially modulated TPL of a Si–Au core–shell nanowire with a 40 nm Au shell. Scale bar is  $1 \mu\text{m}$ .

under a far field condition is reported here for the first time. For Si–Au core–shell nanowires with a 40 nm core, 15 nm Au shell, and lengths ranging between 2.8 and 5.7  $\mu\text{m}$ , patterns with 5 bright peaks were observed. Figure 3a shows 12 TPL images taken from these wires. The mode spacing, defined as the average distance between two adjacent bright spots and measured from the intensity profile along the nanowire axis, is found to increase when increasing the lengths of the wires. By plotting the mode spacing as a function of the wire length, we further confirm that the mode spacing is linearly proportional to the length of the nanowires (Figure 3b), with a slope of  $0.238 \pm 0.003$ .

To probe the impact of the Au shell thickness on the spatially modulated TPL signal, we prepared and tested Si–Au core–shell nanowires with 40 nm Au shells. These nanowires exhibited very similar TPL patterns with 5 bright dots compared to wires with 15 nm Au shell and similar lengths. A representative image is shown in the inset of Figure 4. Furthermore, the mode spacing measured from 6 nanowires with a 40 nm Au layer also showed a linear dependence on the length of the nanowires (Figure 4), with a slope of  $0.239 \pm 0.001$ .

To further characterize the spatially modulated TPL signal, we measured the dependence of its intensity on the excitation wavelength and polarization of the incident laser. We recorded the TPL images of the same sample with sequential excitation of 850, 790, 900, and 850 nm again. Excitation beams were polarized along the wire axis. TPL images show almost identical signal patterns and intensities, which are independent of the excitation wavelength (Figure 5a). When imaging the sample with the different laser polarization, we found that the absolute signal intensity is minimized when the polarization is perpendicular to the nanowire axis and maximized when in the parallel case. However, patterning remains the same, as shown in Figure 5b. A detailed quantitative analysis of intensities as a function of excitation polarization is shown in Figure 5c. Red squares and blue triangles are intensity data taken from the center bright and the adjacent dark spots in Figure 5b, respectively, which were also the center peak and adjacent dip in the intensity line profile. Both intensity data can be fitted to a  $\cos^2$  function indicated by the dash fitting curves. This polarization dependence is consistent with the TPL measurement from gold nanorods by Imura et al.<sup>10</sup> and can be attributed to a sequential two-photon excitation process described by the same group. In this process, the first photon excites a free electron from the sp

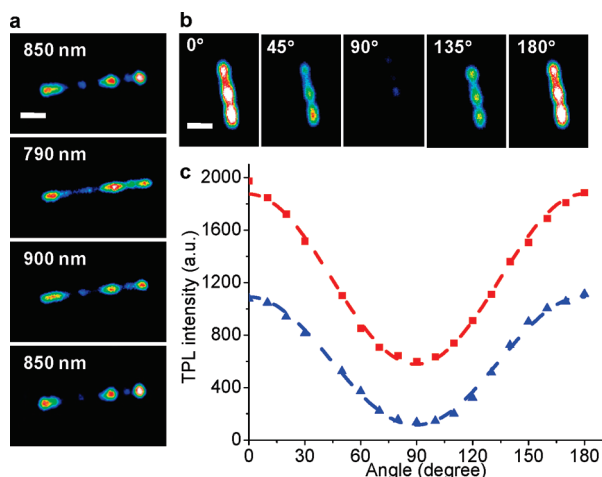


**Figure 5.** Dependence of TPL on excitation wavelength and laser polarization. (a) TPL images with different excitation wavelengths. (b) TPL images with various laser polarizations. Angles between the wire axis and the polarization of laser beam are indicated. (c) TPL intensity as a function of polarization angle. Red and blue represent the TPL intensities taken from the bright and dark spots, respectively. Dashed curves are fitting curves. Scale bars are 1  $\mu\text{m}$ .

band below the Fermi surface to the sp band above the Fermi surface. This transition is resonant with photons with a polarization along the axis of the nanowires. The second photon excites a free electron from the d band to the sp conduction band, this sequential transition is not sensitive to the polarization, and thus the TPL shows a  $\cos^2$  dependence on the laser polarization.

The spatially modulated TPL signal observed in our study is a strong indication of standing waves of surface plasmon polaritons (SPP) along the Si–Au core–shell nanowire. By treating the nanowire as a plasmon Fabry–Pérot resonator, the resonance condition is described by Søndergaard et al.<sup>24</sup>

$$L \frac{2\pi}{\lambda} n = m\pi - \phi \quad (1)$$

where  $L$  is the length of the wire,  $\lambda$  is the SPP wavelength,  $n$  is the real part of mode effective index,  $m$  is an integer representing the order of the resonance, and  $\phi$  is the phase representing the reflection of SPP at the wire termination. For high-order resonances, the effect of  $\phi$  is negligible.<sup>25</sup> For thin gold films, the value of  $n$  is close to 1.0.<sup>26</sup> Under these approximations, eq 1 is simplified into

$$\frac{\lambda}{2L} = \frac{1}{m} \quad (2)$$

According to the standing wave model, the mode spacing should be equal to one-half of the resonance wavelength  $\lambda$ . Therefore, the left side of eq 2 is virtually the slope of the linear curves shown in Figure 3b and Figure 4. For observed TPL patterns with  $m = 4$ , eq 2 predicts a slope of 0.25, which is close to the measured value of 0.238 for nanowires of 15 nm Au shell and 0.239 for nanowires of 40 nm Au shell. Together, our experimental results and modeling indicate that the core–shell nanowires can be treated as a plasmon resonator and that TPL provides a good readout of the plasmonic waves.

## CONCLUSIONS

In summary, we demonstrated a new strategy synthesizing Si/Au core–shell nanowires. This strategy, combining chemical vapor

deposition and wet chemistry methods, will enable metal nanostructure with a smooth surface, a unique geometry, and complete control of key parameters such as core diameter, shell thickness, and nanowire lengths. Significantly, distinguished from a previous TPL study of gold rods several hundred nanometers in length, we observed a spatially modulated TPL from Si–Au core–shell nanowires prepared, of which the lengths are several micrometers. We also demonstrated that the mode spacing is linearly scaled with the length of the wire and can be explained by a standing wave model of the surface plasmon wave. Our results suggest Si–Au core–shell nanowires as a new system for the study of a plasmonic wave in a 1-D nanostructure.

## AUTHOR INFORMATION

### Corresponding Author

\*E-mail: (J.-X.C.)jcheng@purdue.edu, (C.Y.) yang@purdue.edu.

## ACKNOWLEDGMENT

The work was supported by NSF Grant CBET 082883 to J.-X.C. and NSF CAREER award DMR087523 to C.Y.

## REFERENCES

- (1) Mooradian, A. Photoluminescence of Metals. *Phys. Rev. Lett.* **1969**, *22* (5), 185.
- (2) Boyd, G. T.; Yu, Z. H.; Shen, Y. R. Photoinduced Luminescence from the Noble Metals and its Enhancement on Roughened Surfaces. *Phys. Rev. B* **1986**, *33* (12), 7923.
- (3) El-Sayed, M. A. Some Interesting Properties of Metals Confined in Time and Nanometer Space of Different Shapes. *Acc. Chem. Res.* **2001**, *34*, 257–264.
- (4) Wang, H.; Huff, T. B.; Zweifel, D. A.; He, W.; Low, P. S.; Wei, A.; Cheng, J.-X. In vitro and In vivo Two-photon Luminescence Imaging of Single Gold Nanorods. *Proc. Natl. Acad. Sci. U.S.A.* **2005**, *102* (44), 15752–15756.
- (5) Park, J.; Estrada, A.; Sharp, K.; Sang, K.; Schwartz, J. A.; Smith, D. K.; Coleman, C.; Payne, J. D.; Korgel, B. A.; Dunn, A. K.; Tunnell, J. W. Two-photon-induced Photoluminescence Imaging of Tumors Using Near-infrared Excited gold nanoshells. *Opt. Express* **2008**, *16* (3), 1590–1599.
- (6) Kim, H.; Xiang, C.; Guell, A. G.; Penner, R. M.; Potma, E. O. Tunable Two-Photon Excited Luminescence in Single Gold Nanowires Fabricated by Lithographically Patterned Nanowire Electrodeposition. *J. Phys. Chem. C* **2008**, *112* (33), 12721–12727.
- (7) Ghenuche, P.; Cherukulappurath, S.; Taminiau, T. H.; Hulst, N. F. v.; Quidant, R. Spectroscopic Mode Mapping of Resonant Plasmon Nanoantennas. *Phys. Rev. Lett.* **2008**, *101*, 116805.
- (8) Schuck, P. J.; Fromm, D. P.; Sundaramurthy, A.; Kino, G. S.; Moerner, W. E. Improving the Mismatch between Light and Nanoscale Objects with Gold Bowtie Nanoantennas. *Phys. Rev. Lett.* **2005**, *94* (1), 017402.
- (9) Imura, K.; Nagahara, T.; Okamoto, H. Plasmon Mode Imaging of Single Gold Nanorods. *J. Am. Chem. Soc.* **2004**, *126* (40), 12730–12731.
- (10) Imura, K.; Nagahara, T.; Okamoto, H. Near-Field Two-Photon-Induced Photoluminescence from Single Gold Nanorods and Imaging of Plasmon Modes. *J. Phys. Chem. B* **2005**, *109* (27), 13214–13220.
- (11) Ditlbacher, H.; Hohenau, A.; Wagner, D.; Kreibitz, U.; Rogers, M.; Hofer, F.; Aussenegg, F. R.; Krenn, J. R. Silver Nanowires as Surface Plasmon Resonators. *Phys. Rev. Lett.* **2005**, *95* (25), 257403.
- (12) Dorfmueller, J.; Vogelgesang, R.; Weitz, R. T.; Rockstuhl, C.; Etrich, C.; Pertsch, T.; Lederer, F.; Kern, K. Fabry–Pérot Resonances in One-Dimensional Plasmonic Nanostructures. *Nano Lett.* **2009**, *9*, 2372–2377.

- (13) Graff, A.; Wagner, D.; Ditlbacher, H.; Kreibig, U. Silver nanowires. *Eur. Phys. J. D* **2005**, *34*, 263–269.
- (14) Stefan, A. M.; Harry, A. A. Plasmonics: Localization and guiding of electromagnetic energy in metal/dielectric structures. *J. Appl. Phys.* **2005**, *98* (1), 011101.
- (15) Verhagen, E.; Spasenovic, M.; Polman, A.; Kuipers, L. Nano-wire Plasmon Excitation by Adiabatic Mode Transformation. *Phys. Rev. Lett.* **2009**, *102* (20), 203904.
- (16) Schider, G.; Krenn, J. R.; Hohenau, A.; Ditlbacher, H.; Leitner, A.; Aussenegg, F. R.; Schaich, W. L.; Puscasu, I.; Monacelli, B.; Boreman, G. Plasmon dispersion relation of Au and Ag nanowires. *Phys. Rev. B* **2003**, *68* (15), 155427.
- (17) Falk, A. L.; Koppens, F. H. L.; Yu, C. L.; Kang, K.; de Leon Snapp, N.; Akimov, A. V.; Jo, M.-H.; Lukin, M. D.; Park, H. Near-field electrical detection of optical plasmons and single-plasmon sources. *Nat. Phys.* **2009**, *5* (7), 475–479.
- (18) Sanders, A. W.; Routenberg, D. A.; Wiley, B. J.; Xia, Y.; Dufresne, E. R.; Reed, M. A. Observation of Plasmon Propagation, Redirection, and Fan-Out in Silver Nanowires. *Nano Lett.* **2006**, *6* (8), 1822–1826.
- (19) Cui, Y.; Lauhon, L.; Gudixsen, M.; Wang, J.; Lieber, C. Diameter-controlled synthesis of single-crystal silicon nanowires. *Appl. Phys. Lett.* **2001**, *78*, 2214–2216.
- (20) Brinson, B. E.; Lassiter, J. B.; Levin, C. S.; Bardhan, R.; Mirin, N.; Halas, N. J. Nanoshells Made Easy: Improving Au Layer Growth on Nanoparticle Surfaces. *Langmuir* **2008**, *24* (24), 14166–14171.
- (21) Pham, T.; Jackson, J. B.; Halas, N. J.; Lee, T. R. Preparation and Characterization of Gold Nanoshells Coated with Self-Assembled Monolayers. *Langmuir* **2002**, *18* (12), 4915–4920.
- (22) Duff, D. G.; Baiker, A.; Edwards, P. P. A new hydrosol of gold clusters. 1. Formation and particle size variation. *Langmuir* **1993**, *9* (9), 2301–2309.
- (23) Chen, H.; Wang, H.; Slipchenko, M. N.; Jung, Y.; Shi, Y.; Zhu, J.; Buhman, K. K.; Cheng, J.-X. A multimodal platform for nonlinear optical microscopy and microspectroscopy. *Opt. Express* **2009**, *17* (3), 1282–1290.
- (24) Søndergaard, T.; Bozhevolnyi, S. Slow-plasmon resonant nanostructures: Scattering and field enhancements. *Phys. Rev. B* **2007**, *75*, 073402.
- (25) Søndergaard, T.; Beermann, J.; Boltasseva, A.; Bozhevolnyi, S. I. Slow-plasmon resonant-nanostructure antennas: analysis and demonstration. *Phys. Rev. B* **2008**, *77*, 115420.
- (26) Bozhevolnyi, S.; Søndergaard, T. General properties of slow-plasmon resonant nanostructures: nano-antennas and resonators. *Opt. Express* **2007**, *17*, 10869.